ISIJ International, Vol. 43 (2003), No. 8, pp. 1238–1243

Development of Hard Bainite

C. GARCIA-MATEO, F. G. CABALLERO[1)] and H. K. D. H. BHADESHIA

University of Cambridge, Department of Materials Science and Metallurgy, Pembroke Street, Cambridge CB2 3QZ, UK. 1) Centro Nacional de Invesigaciones Metalurgicas (CENIM), Consejo Superior de Investiaciones Cientificas (CSIC), Avda. Gregorio del Amo, 8, 28040 Madrid, Spain.

(*Received on October 28, 2002; accepted in final form on February 10, 2003*)

It is demonstrated that in a high-carbon steel where carbide precipitation is suppressed, bainite can be obtained by isothermal transformation at temperatures as low as 200°C. The time taken for nucleation at this temperature can be many days, but the transformation results in the growth of extremely thin platelets of bainite, so thin that the hardness of the resulting steel can be greater than 600 HV.

KEY WORDS: bainite; steel; hardness; phase transformations.

1. Introduction

The T_0 temperature in steel is defined as that at which ferrite and austenite of the same chemical composition have identical free energy. The T_0' temperature is that below which it is possible for austenite to transform to ferrite of the same chemical composition after allowing for the strain energy due to the displacements associated with the transformation. Bainite is expected below the T_0' temperature when:

$$\Delta G^{\gamma\to\alpha} < -G_{SB} \quad \text{and} \quad \Delta G_m < G_N \qquad (1)$$

where $G_{SB} \simeq 400\,\mathrm{J\,mol^{-1}}$ is the stored energy of bainite (α)[1)]; $\Delta G^{\gamma\to\alpha}$ is the free energy change accompanying the transformation of austenite (γ) without any change in chemical composition. The first condition therefore describes the limits to growth. The second condition refers to nucleation; thus, ΔG_m is the maximum molar Gibbs free energy change accompanying the nucleation of bainite.[2)]

G_N is a universal function based on a dislocation mechanism of nucleation rather than classical theory which relies on heterophase fluctuations.[1–3)] The temperature dependence of G_N is, for low-alloy steels, independent of chemical composition; together with the growth condition, the function allows the calculation of the bainite-start temperature from a knowledge of thermodynamics alone.[1,2)]

In a similar scheme, martensitic transformation becomes possible when[4–9)]

$$\Delta G^{\gamma\to\alpha}\{M_S\} < G_N^{\alpha'} \qquad (2)$$

where the right hand side of this equation refers to the critical value of $\Delta G^{\gamma\to\alpha}$ needed to stimulate martensite by an athermal, diffusionless nucleation and growth mechanism.[3)]

It is possible, using Eqs. (1) and (2) to calculate the bainite-start (B_S) and martensite-start (M_S) temperatures as a function of steel composition. A set of these calculations for a steel with sufficient hardenability to avoid other transformations are illustrated in **Fig. 1**(a). From a thermodynamic point of view, it clearly is possible to obtain bainite at very low temperatures. To estimate whether this is a reasonable statement from a kinetic point of view, time–temperature–transformation (TTT) diagrams were calculated as described elsewhere.[10,11)] The time required to initiate transformation just below B_S is plotted in Fig. 1(b) as a function of the carbon concentration; it takes approximately a year to begin forming bainite when the carbon concentration of the Fe–2Si–3Mn alloy reaches 1 wt%, and at somewhat higher concentrations reaches 10 years. Therefore, there is a severe kinetic limitation to producing bainite in such a steel for temperatures below about 400 K. It was our aim to produce

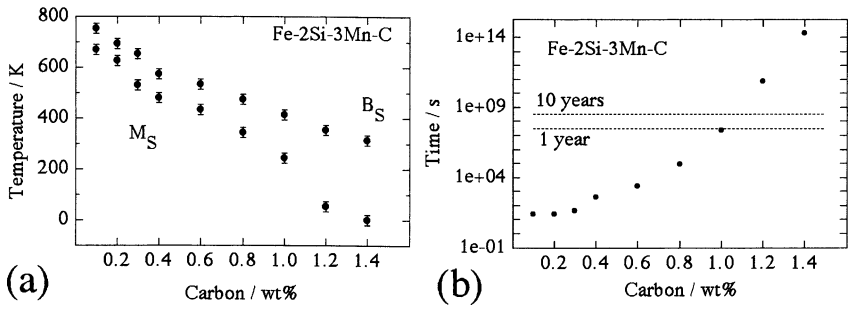

Fig. 1. Calculated transformation temperatures and times to initiate transformation at B_S as a function of the carbon concentration. The calculations were carried out as in Refs. 10),11).

Table 1. Chemical composition and martensite-start temperature.

C	Si	Mn	Mo	Cr	V	P wt%	M_S / °C
0.98	1.46	1.89	0.26	1.26	0.09	< 0.002	120

bainite at a low temperature in a steel designed for a specific structural application.[12)]

2. Experimental Techniques

The chemical composition of the alloy, measured after homogenisation at 1 200°C for 2 d whilst sealed in a quartz capsule containing pure argon, is given in **Table 1**. During processing, it is important to ensure that the cooling rate from 1 200°C to ambient temperature is slow enough to avoid martensitic transformation since the high-carbon martensite plates tend to crack spontaneously, permanently compromising the integrity of the sample. The cooling from 1 200°C was therefore accomplished by switching off the furnace to obtain pearlite as the microstructure at ambient temperature.

The procedure of protecting samples against oxidation by sealing in quartz tubes was used for all heat treatments, including austenitisation at 1 000°C for 15 min prior to isothermal transformation at temperatures in the range 125–325°C. The martensite-start temperature was determined experimentally on a 2 mm diameter rod using high-speed dilatometry.

X-ray experiments were conducted using a Philips PPW1730 diffractometer and a scanning rate (2θ) of 1 °min^{-1}, with unfiltered Cu $K\alpha$ radiation. The system was operated at 45 kV and 45 mA. The retained austenite content was calculated using integrated intensities of the 200, 220 and 311 austenite peaks and the 002, 112 and 022 peaks of ferrite. Using this number of peaks avoids possible bias due to crystallographic texture.[13)] The carbon concentrations of the austenite and bainitic ferrite were estimated from their lattice parameters, using equations published elsewhere.[14)]

Specimens for transmission electron microscopy were machined from 3 mm diameter rods which were sliced into 100 μm discs. These were ground down to 50 μm thickness using 1 200 grit silicon carbide paper, for electropolishing at 50 V using a twin-jet unit. The electrolyte consisted of 5% perchloric acid, 15% glycerol and 80% methanol. A JEOL JEM-200CX transmission electron microscope operated at 200 kV was used to examine the thin foils.

The martensite-start temperature (M_S) was determined using an Adamel Lhomargy DT1000 high-resolution dilatometer using cylindrical specimens 12 mm length and 2 mm diameter. The samples were heated to 1 000°C at 5°C s^{-1} and then forced to cool using helium at either 100 or 200°C s^{-1}. There was no perceptible difference between the M_S temperature measured at these two cooling rates.

3. Results and Discussion

3.1. Alloy Design

The alloy contains manganese, vanadium and chromium for hardenability, silicon to prevent the precipitation of cementite during upper bainite formation and molybdenum to prevent temper embrittlement due to phosphorus. The carbon concentration was selected using calculations of the type illustrated in Fig. 1, to suppress B_S whilst at the same time have realistic transformation times. The extent of transformation was followed using hardness and optical microscopy; experimental data are listed in **Table 2**. Note that only minute quantities of bainite were observed after prolonged transformation at 125 and 150°C.

Table 2. Approximate times corresponding to the cessation of the bainite reaction at the temperatures indicated.

Transformation temperature / °C	125	150	200	250	300	325
Time for end of reaction / days	>60	>30	9	3–4	1–2	1–2

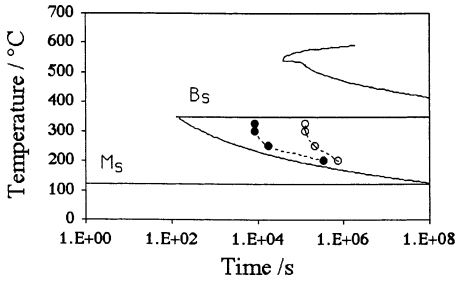

Fig. 2. Calculated TTT diagram for the initiation of isothermal reaction. The upper C-curve represents the onset of reconstructive transformations such as allotriomorphic ferrite and pearlite, whereas the lower curve is for bainite.[10,11)] The filled points represent the measured start of the bainite reaction and the open circles where the reaction stops.

3.2. Kinetics

The calculated[10,11)] transformation temperatures and TTT diagram are shown in **Fig. 2**, which also contains experimental data for the time taken to initiate and cease transformation. The measured values for the achievement of a detectable degree of transformation are in reasonable agreement with those calculated (Fig. 2), except at the highest temperature where the time period required is underestimated.

Figure 3 shows a typical set of optical micrographs to illustrate the evolution of the transformation at 250°C.

3.3. Hardness and Phase Fractions

It is useful first to discuss the hardness and microstructures obtained at the longest time intervals, when transformation essentially ceases. X-ray analysis and metallography showed that at that point, the microstructure consisted of a mixture of just two phases, bainitic ferrite and carbon-enriched retained austenite (**Fig. 4**). The ultimate hardness increases sharply as the transformation temperature is reduced, even though the corresponding fraction of bainitic ferrite only increases from about 0.5 to 0.7 over the same temperature range. As will be seen later, the increase in hardness is because the thickness of the bainite plates decreases sharply as the transformation temperature is re-

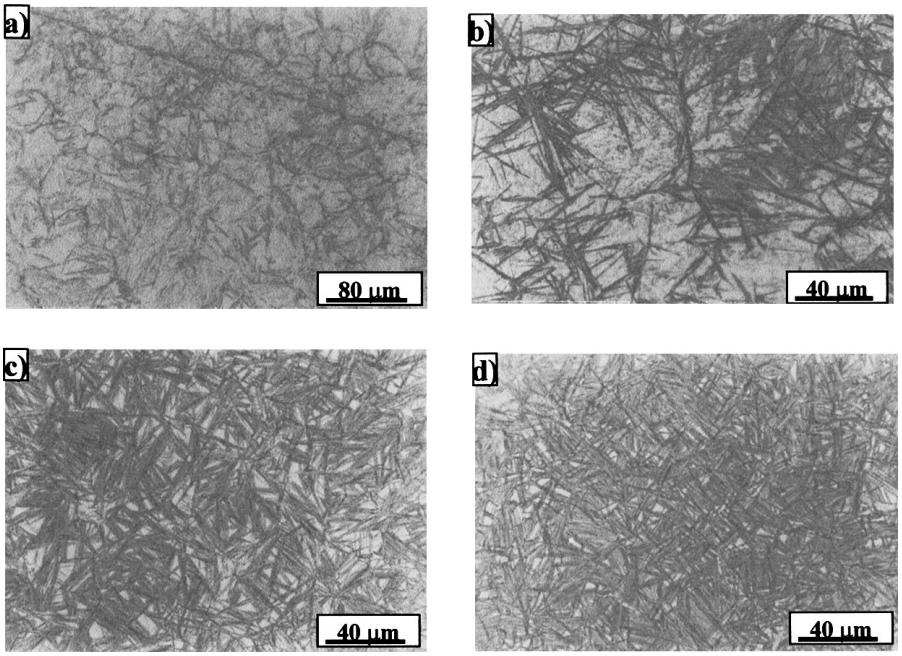

Fig. 3. Optical micrographs of bainite obtained by isothermal transformation at 250°C. The reaction times and hardness values are (a) 1 h, 590 HV; (b) 24 h, $V_b \simeq 0.34$, 391 HV; (c) 2 d, $V_b \simeq 0.58$, 521 HV; (d) 15 d, $V_b \simeq 0.64$, 550 HV.

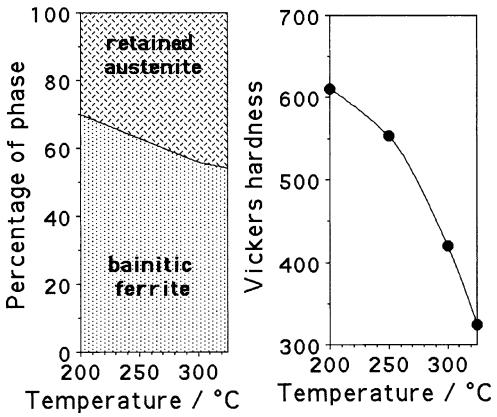

Fig. 4. Phase fractions determined as described in the text, and hardnesses (HV30) of the microstructure obtained by prolonged isothermal transformation.

duced.

The detailed variation of hardness as a function of time and temperature is illustrated in **Fig. 5**. Each hardness point on the graphs represents a mean of three measurements with a typical variation of only ±7 HV. The actual scatter illustrated in Fig. 5 is larger, particularly at small fractions of transformation. Each data point illustrated is from measurements on a different sample. Since the heat treatment conditions were controlled to better than ±5°C, and since the alloy had been processed and homogenised prior to the heat treatments, it is concluded that the variation is due to the stochastic nature of the nucleation process, and is particularly noticeable because of the slow rate of transformation.

The hardness of the as-quenched microstructure is illustrated as a horizontal band on each diagram; this microstructure is a mixture of retained austenite and martensite and the width of the bands is indicative of variations in their fractions. Similarly, there is more scatter in the data at the early stages of transformation when the microstructures are a mixture of bainite, martensite and retained austenite.

In normal low-carbon low-alloy steels the hardness decreases continuously as transformation progresses, from that of a fully martensitic state to that of a predominantly bainitic microstructure. This is indeed the general trend evident for transformation at 325 and 300°C (Fig. 5). However, large minima occur in the plots for 250 and 200°C. This is because the hardness first decreases as bainite replaces martensite, but as the fraction of fine-bainite increases, so does the hardness. Indeed the ultimate hardness of the mixture of fine-bainitic ferrite and austenite reaches very high levels comparable to the mixture of martensite and austenite at zero transformation time. The effect only appears at the lower transformation temperatures because, as discussed later, the microstructure then becomes highly refined.

The experiments demonstrate that it is possible to obtain bainitic microstructures which have a hardness in excess of 600 HV.

3.4. Incomplete Reaction

As is well known,[2] the presence of silicon prevents the complete transformation of austenite because the reaction to bainite stops when the chemical composition of the austenite violates the growth condition described in Eq. (1). Thus, the completion of transformation leaves carbon-enriched residual austenite which can no longer transform into bainite. The carbon concentrations of the austenite and bainite, determined using standard X-ray analysis are presented in **Fig. 6** for the samples in which the transformation had stopped. The equations used to convert lattice parameters into concentration for both ferrite and austenite, are from Ref. 14). The T_0' and the paraequilbrium $\alpha+\gamma/\gamma$ phase boundaries were calculated using the commercially available MTDATA program and the SGTE database.

As expected from the incomplete-reaction phenomenon,[2] the carbon concentration of austenite at the point

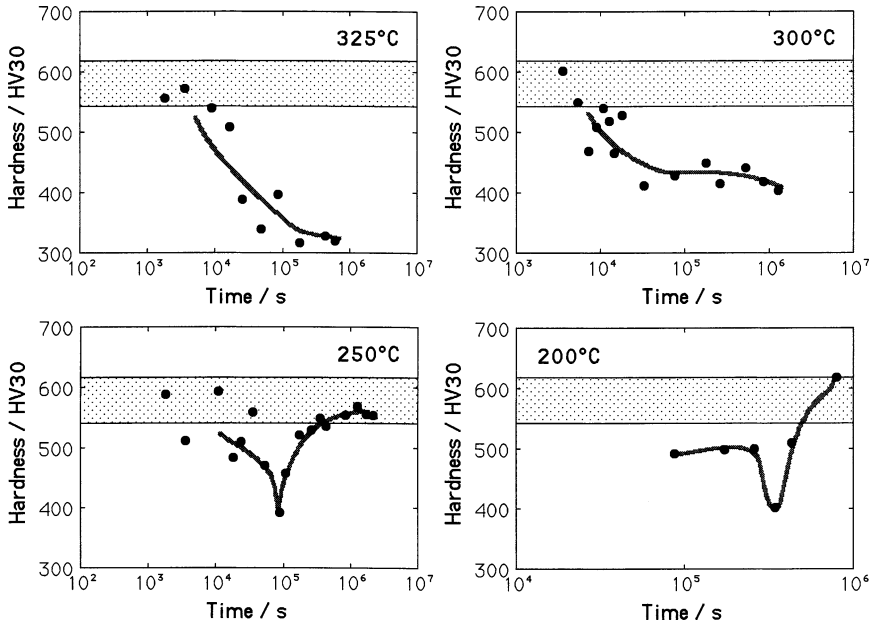

Fig. 5. Vickers hardness as a function of the isothermal transformation temperature and time. The shaded bands represent the hardness of a mixture of martensite and austenite obtained by water quenching from a fully austenitic state. Note that for clarity, the time scale for T=200°C is different from the other graphs.

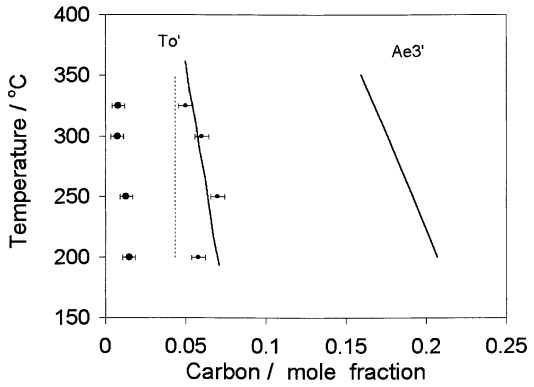

Fig. 6. A comparison of experimental data against calculated T_0' and Ae_3' phase boundaries. The larger points on the left are the measured mole fractions of carbon in bainitic ferrite, and the smaller points on the right represent the carbon concentrations of austenite. The dashed vertical line represents the average mole fraction of carbon in the alloy.

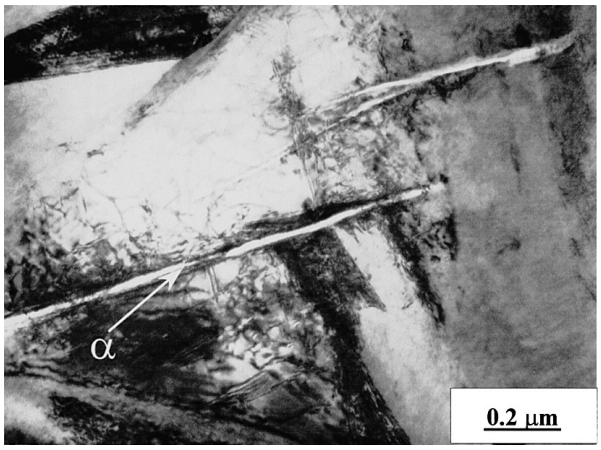

Fig. 7(a). Transformed at 200°C for 4 d. The initiation time for this reaction is about 4 d.

where the reaction terminates is far less than demanded by equilibrium (Ae_3'), and close to that expected from the T_0' phase boundary after allowing for the heterogeneous distribution of carbon.[2] An interesting feature is that significant excess quantities of carbon are retained in solution within the bainitic ferrite; it is speculated that the carbon may be trapped at defects.[15,16]

Selected transmission electron micrographs are presented in **Fig. 7**. Some of the plates of bainite are incredibly thin and long, giving a most elegant fine-scale structure consisting of an intimate mixture of austenite and ferrite. Dislocation debris is evident in both the bainitic ferrite and the surrounding austenite. Extensive transmission microscopy failed to reveal carbides, presumably because of the high silicon concentration. Thus, features intruding into the plate of bainite on the top right-hand side in Fig. 7(b) were verified using electron diffraction and dark-field imag-

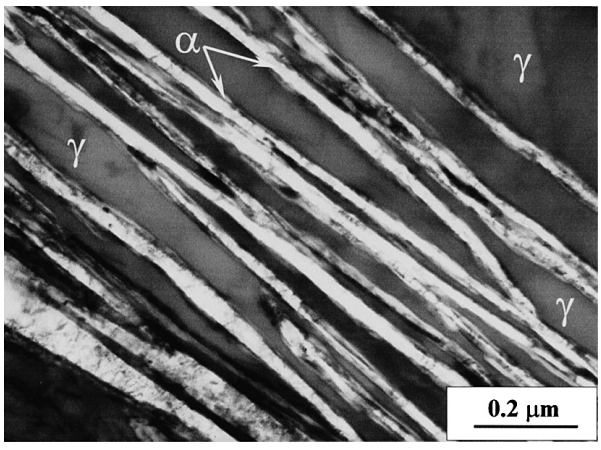

Fig. 7(b). Transformed at 200°C for 5 d.

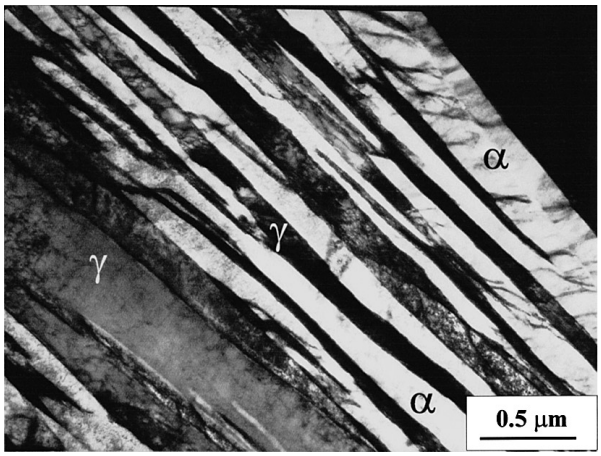

Fig. 7(c). Transformed at 250°C for 30 h.

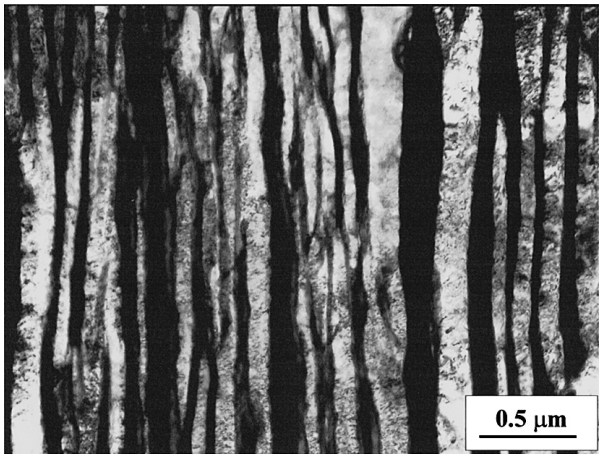

Fig. 7(d). Transformed at 250°C for 25 d.

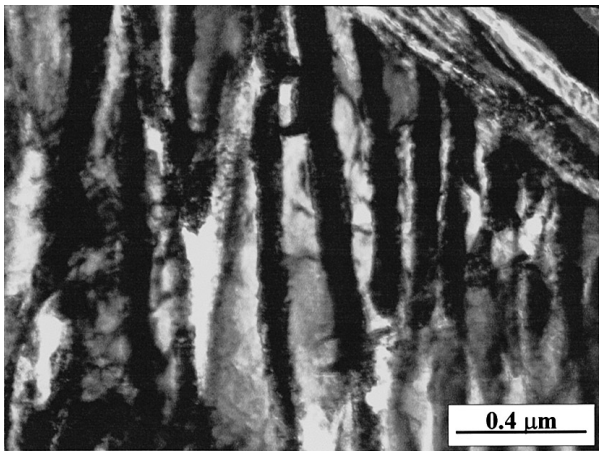

Fig. 7(e). Bright field image of sample transformed at 200°C for 15 d.

ing to be films of retained austenite rather than carbides.

The scale of the bainite plates as measured using transmission electron microcopy, and correcting for stereological effects[17] is illustrated as a function of transformation temperature in **Fig. 8**; the uncertainties in the measurements are estimated from the numbers of measurements conducted in each case. It is the very small thickness which leads to hardnesses in excess of 600 HV.[2] For a given thick-

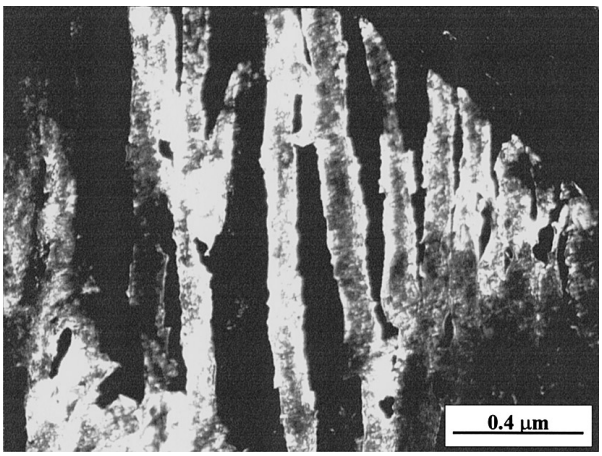

Fig. 7(f). Dark field image corresponding to Fig. 7(e), of sample transformed at 200°C for 15 d. The image was obtained using an 002_γ reflection.

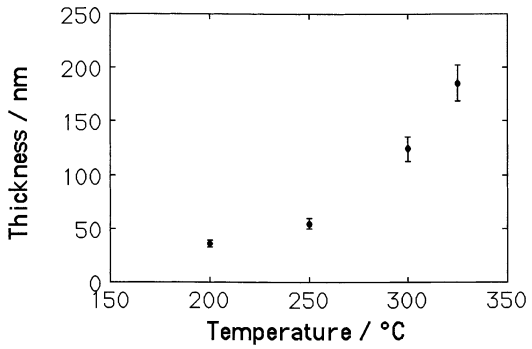

Fig. 8. Stereologically corrected thickness of bainite plates as a function of the transformation temperature.

ness t, the mean lineal intercept overline $\bar{L} \simeq 2t$,[18,19] and the strength contribution due to the size of the plates is given by $\Delta\sigma = 115(\bar{L})^{-1}$ MPa where $\bar{L}$ is in micrometers.[20,21] It follows that $\Delta\sigma \simeq 311$ MPa for plates of thickness 185 nm obtained by transformation at 325°C, whereas $\Delta\sigma \simeq 1\,642$ MPa for plates of thickness 35 nm obtained by transformation at 200°C.

4. Summary

It has been possible to achieve bainitic transformation at temperatures as low as 200–125°C, where the calculated diffusion distance of an iron atom is inconceivably small over the time period of the experiments. The transformation can only be achieved via a displacive transformation mechanism. Furthermore, the scale of the microstructure achieved is very fine indeed, amounting to tens of nanometers, an observation consistent with the very high hardness values of microstructures which are mixtures of only bainitic ferrite and carbon-enriched austenite. Indeed, hardness values in excess of 600 HV are reported for microstructures which contain only bainitic ferrite and retained austenite.

There are detailed observations which remain to be explained: for example, the fact that excess carbon is retained in solid solution and that it does not precipitate during prolonged heat treatment. A possible reason for the lack of carbide precipitation is that the excess carbon in ferrite is

trapped at defects, where its energy is lower than in the precipitate phase. These topics are the subject of research in progress.

Acknowledgments

We would like to acknowledge the Engineering and Physical Sciences Research Council (U.K.) and the U.K. Ministry of Defence for funding this work. Dr F. G. Caballero would like to thank the Dirección General de Investigación de la Comunidad Autnoma de Madrid (CAM) for the financial support in the form of a postdoctoral research grant.

REFERENCES

1) H. K. D. H. Bhadeshia; *Acta. Metall.* **29** (1981), 1117.
2) H. K. D. H. Bhadeshia: Bainite in Steels, 2nd ed., Institute of Materials, London, (2001), 134.
3) G. B. Olson and M. Cohen: *Metall. Trans*. *A*, **7A** (1976), 1897.
4) L. Kaufman and M. Cohen: *Progress in Metal Physics*, **7** (1958), 165.
5) Y. Imai, M. Izumiyama and M. Tsuchiya: *Sci. Rep. Res. Inst. Tohoku Univ.*, **A17** (1965), 173.
6) H. K. D. H. Bhadeshia: *Met. Sci.*, **15** (1981), 175.
7) H. K. D. H. Bhadeshia: *Met. Sci.*, **15** (1981), 178.
8) G. Ghosh and G. B. Olson: *Acta Metall*. *Mater.*, **42** (1994), 3361.
9) T. Cool and H. K. D. H. Bhadeshia: *Mater. Sci*. *Technol*., **12** (1996), 40.
10) H. K. D. H. Bhadeshia: *Met. Sci.*, **16** (1982), 159.
11) J.-L. Lee and H. K. D. H. Bhadeshia: *Mater. Sci*. *Eng. A*, **A171** (1993), 223.
12) F. G. Caballero, H. K. D. H. Bhadeshia, K. J. A. Mawella, D. G. Jones and P. Brown: *Mater. Sci*. *Technol*., **18** (2002), 279.
13) M. J. Dickson: *J. Appl. Crystallogr.*, **2** (1969), 176.
14) H. K. D. H. Bhadeshia, S. A. David, J. M. Vitek and R. W. Reed: *Mater. Sci*. *Technol*., **7** (1991), 686.
15) H. K. D. H. Bhadeshia and A. R. Waugh: Proc. of the Int. Solid–Solid Phase Transformations Conf., The Metallurgical Society of the AIME, Warrendale, PA, (1981), 993.
16) H. K. D. H. Bhadeshia and A. R. Waugh: *Acta. Metall.,* **30** (1982) 775.
17) L.-C. Chang and H. K. D. H. Bhadeshia: *Mater. Sci. Technol.*, **11** (1995), 874.
18) C. Mack: *Proc. Cambridge Philosophical Society*, **52** (1956), 246.
19) H. K. D. H. Bhadeshia: Mathematical Modelling of Weld Phenomena III, Institute of Materials, London, (1997), 229.
20) G. Langford and M. Cohen: *Trans*. *Am. Soc, Met.*, **62** (1969), 623.
21) G. Langford and M. Cohen: *Metall. Mater. Trans*., **1** (1970), 1478.